**Atmospheric
Chemistry
and Physics
Discussions**

Multi-scale modeling study of the source contributions to near-surface ozone and sulfur oxides levels over California during the ARCTAS-CARB period

M. Huang[1], G. R. Carmichael[1], S. N. Spak[1], B. Adhikary[1,2], S. Kulkarni[1], Y. F. Cheng[1], C. Wei[1], Y. Tang[3], A. D'Allura[4], P. O. Wennberg[5], G. L. Huey[6], J. E. Dibb[7], J. L. Jimenez[8], M. J. Cubison[8], A. J. Weinheimer[9], A. Kaduwela[10], C. Cai[10], M. Wong[11], R. B. Pierce[12], J. A. Al-Saadi[13], D. G. Streets[14], and Q. Zhang[14]

[1]Center for Global and Regional Environmental Research, the University of Iowa, Iowa City, IA, USA
[2]Kathmandu University, Dhulikhel, Nepal
[3]Meso-scale modeling, NOAA/NCEP/EMC, W/NP2, NOAA, Camp Springs, MD, USA
[4]ARIANET Srl, Milano, Italy

ACPD

10, 27777–27823, 2010

Ozone and sulfur oxides levels over California

M. Huang et al.

Title Page

Abstract	Introduction
Conclusions	References
Tables	Figures

◄◄   ►►

◄   ►

Back   Close

Full Screen / Esc

Printer-friendly Version

Interactive Discussion

[5] California Institute of Technology, Pasadena, CA, USA
[6] Geogia Institute of Technology, Atlanta, GA, USA
[7] University of New Hampshire, Durham, NH, USA
[8] University of Colorado, Boulder, CO, USA
[9] NCAR, Boulder, CO, USA
[10] California Air Resource Board, Sacramento, CA, USA
[11] The University of Maryland, MD, USA
[12] NOAA/NESDIS, Madison, WI, USA
[13] NASA Langley Research Center, Hampton, VA, USA
[14] Argonne National Laboratory, Argonne, IL, USA

Correspondence to: M. Huang (mhuang1@engineering.uiowa.edu)

Ozone and sulfur oxides levels over California

M. Huang et al.

Title Page

Abstract	Introduction
Conclusions	References
Tables	Figures

|◄ | ►|

◄ | ►

| Back | Close |

Full Screen / Esc

Printer-friendly Version

Interactive Discussion

Abstract

Chronic ozone (O_3) problems and the increasing sulfur oxides ($SO_x = SO_2 + SO_4$) ambient concentrations over South Coast (SC) and other areas of California (CA) are affected by both local emissions and long-range transport. In this paper, multi-scale tracer and full-chemistry simulations with the STEM atmospheric chemistry model are used to assess the contribution of local emission sources to SC O_3 and evaluate the impacts of transported sulfur and local emissions on the SC sulfur budget during the ARCTAS-CARB experiment period in 2008. Sensitivity simulations quantify contributions of biogenic and fire emissions to SC O_3 levels. California biogenic and fire emissions contribute 3–4 ppb to near-surface O_3 over SC, with larger contributions to other regions in CA. Long-range transport from Asia is estimated to enhance surface SO_4 over SC by $\sim$0.5 µg/sm^3, and the higher SO_x levels (up to $\sim$0.7 ppb of SO_2 and $\sim$6 µg/sm^3 of SO_4) observed above $\sim$6 km did not affect surface air quality in the study region. Enhanced near-surface SO_x levels over SC during the flight week were attributed mostly to local emissions. Two anthropogenic SO_x emission inventories (EIs) from the California Air Resources Board (CARB) and the US Environmental Protection Agency (EPA) are compared and applied in 60 km and 12 km chemical transport simulations, and the results are compared with observations. The CARB EI shows improvements over the National Emission Inventory (NEI) by EPA, but generally underestimates surface SC SO_x by about a factor of two. Maritime (mostly shipping) emissions contribute to the high SO_2 levels over the ocean and on-shore, and fine SO_4 over the downwind areas is impacted by maritime sources. Maritime emissions also modify the NO_x-VOC limitations over coastal areas. These suggest an important role for shipping emission controls in reducing fine particle and O_3 concentrations in SC.

1 Introduction

In the past 20 years, California population has increased by 33% and the economy has grown rapidly (Cox et al., 2009). In the meanwhile, California has taken good efforts to reduce the emissions of most primary pollutants and the entire state has met the state and national standards for most of these pollutants except troposphere ozone (O_3) and particulate matter (PM). Nearly all Californians live in areas that are designated as nonattainment for the state (about 99%) and national (about 93%) health-based O_3 and/or PM standards.

O_3 is an atmospheric pollutant harmful to human health and agriculture, and is also one of the most important short-lived green-house gases (GHG). The US National Ambient Air Quality Standard (NAAQS) for daily maximum 8-h average O_3 has recently been lowered to 75 ppb, and is likely to be lowered further to between 60 ppb and 70 ppb in future regulatory reviews of its direct impacts on human health. The California Air Resource Board (CARB) currently sets more stringent state 1-h and 8-h O_3 standards at 90 ppb and 70 ppb to better address longstanding urban and regional O_3 problems. Despite the continued precursor emission reductions, limited improvement in O_3 has been achieved over the last decade. Local production from both natural and anthropogenic emission sources, together with inter-continental and in-state transport contributes to the O_3 levels over both urban and rural areas.

Aerosols play an important role in the climate system causing both direct and indirect effects (IPCC report, 2007). They can be transported thousands of kilometers due to their lifetimes of about a week, and adversely affect human health and visibility. Sulfate (SO_4) is an important component of ambient aerosols, and it has a cooling effect on climate. Sulfur compounds emitted into the atmosphere are ultimately oxidized into SO_4, by a variety of oxidants such as hydroxyl radical (OH) and hydrogen peroxide (H_2O_2) in gas and/or liquid phases. Among various sulfur compounds, SO_2 remains an important primary atmospheric pollutant. It is a highly reactive gas harmful to human respiratory system. It can be emitted from both anthropogenic and

natural sources, or can be oxidized from other chemicals such as hydrogen sulfide (H_2S) by OH. SO_2 emissions from anthropogenic sources are generally thought to be better known than other species such as non-methane volatile organic compounds (NMVOCs). The documented largest sources of SO_2 emissions in the US are from fossil fuel combustion at power plants (66%) and other industrial facilities (29%) (US EPA, http://www.epa.gov/air/sulfurdioxide/). Various techniques have been used to control SO_2 emissions from these large sources. However, the major SO_2 emission sources over California vary with location. Unlike the continuous decreasing trend in statewide NO_x, VOC, and CO emissions through the past decades, anthropogenic SO_x emissions started to increase from 2005 and this trend is estimated to continue for the next 10 years. This increasing trend is mainly due to the emissions from the "other mobiles" categories, including the significant growth in shipping activities and the high-sulfur fuels that ocean-going vessels typically use, especially around the coastal areas such as San Francisco (SF) and Los Angeles (LA) counties (Cox et al., 2009). Although shipping emission control regulations are in action since 2009, the SO_2 levels over some South Coast (SC) surface sites are still increasing. In addition, SO_2 emitted from terrestrial industrial processes, certain modes of surface transport, and area sources contribute to the SO_x concentrations over southern California, and similar as O_3 and its precursors, long-range transport of SO_4 affects the California sulfur budget. Because of various health concerns, the US EPA has recently tightened the primary standard for 1-h SO_2 to 75 ppb and changed the SO_2 monitoring requirements.

The design of effective emission reduction strategies requires estimates of the factors that influence the regional background pollution levels and the local enhancements. A number of observational and modeling studies have been conducted to quantify the effects of sector emissions on near-surface O_3 and SO_x levels. It has been concluded that less than 40 ppb of O_3 are contributed by natural sources (Fiore et al., 2003; Wang et al., 2009; Koo et al., 2010). As for anthropogenic emissions, the effects of shipping emissions on regional air quality have been shown important since 1997 (Corbett et al., 1997) over different regions. For example, Vutukuru et al. (2008)

Ozone and sulfur oxides levels over California

M. Huang et al.

focused their studies on the emissions from the LA – Long Beach area, where one third of the cargo containers to the US arrive (BST associates, 2007). They estimated the impacts of shipping emissions on surface 1-h and 8-h O_3 to be up to >20 ppb, and the SO_2 emissions from shipping to cause a rise in on-shore SO_2 concentrations by 2–4 ppb in 2002 and is projected to grow to 8–10 ppb by 2020.

However, the accuracy of observational-based studies of estimating natural O_3 levels relies on the representativeness of measurement sites and the methods to filter out the local anthropogenic contributions (Fiore et al., 2003), and the studies of fire impacts of O_3 are mostly conducted by comparing O_3 levels during fire and non-fire periods, in which way daily variations due to other factors cannot be completely excluded (Viswanathan et al., 2006; Bytnerowicz et al., 2010). Model-based estimations are also uncertain as they are highly dependent on model resolution, key inputs (such as emission inventories (EIs) and meteorology conditions), chemical mechanisms and the study periods (Pfister et al., 2008; Wang et al., 2009; Koo et al., 2010). Many of these modeling studies use coarse grids (from 36 km to several degrees horizontally), and the O_3 enhancement resulting from biogenic and fire sources are estimated either by tracer calculations (Pfister et al., 2008), or from simulations using purely natural emissions (Koo et al., 2010).

As one of the most important model inputs that affect the uncertainties of source contribution studies, EIs have been developed based on various data sources and assumptions, with different spatial and temporal variability. Their reliability needs to be validated. A previous field experiment, the Intercontinental Transport and Chemical Transformation of Anthropogenic Pollution (ITCT), conducted by NOAA in 2002 discovered the potential underestimation in sulfur species emissions (2010 CalNex science and implementation plan, 2008). The uncertainties imported from EIs in source contribution studies need to be quantified. By using two natural EIs (SMOKE and MEGAN), natural O_3 backgrounds differed by 4 ppb in a 2002 case mainly due to differences in lightning emissions but were close in a 2018 case (Koo et al., 2010). Model simulations with different EIs and the comparisons with various three-dimensional observational

datasets are important methods to complement the EI validation and provide better understanding in the uncertainties of source contribution studies.

In this paper we estimate various source contributions to the regional background O_3 levels and local enhancements of SO_x by analyzing observations obtained during the California portion of the Arctic Research of the Composition of the Troposphere from Aircraft and Satellites (ARCTAS-CARB) field experiment period (18 June–24 June 2008) using the STEM regional-scale modeling system, which includes a tracer model and full-chemistry simulations at two different spatial and temporal resolutions. Based on the modeled pollutant spatial patterns and the quantity of flight observational data, we mainly focus this study on California's South Coast (SC) region. We look at the near-surface O_3 and SO_x distributions over SC (and other regions) and identify the effects of long-range transport and local contributions. The long-range transport of O_3 during a specific period has been analyzed in Huang et al. (2010) and the SO_x transport will be discussed in this paper. We quantify the effects of the local emissions from natural sources (i.e., biogenic and wildfires) on O_3 levels with two different EIs in two resolutions, and estimate the impacts of maritime emissions on on-shore air quality in the finer grids. We also compare results using two SO_x EIs with observations and identify areas where further improvements are needed.

2 Methods

2.1 Mission and source data

The ARCTAS-CARB field experiment was conducted in June 2008 by the National Aeronautics and Space Administration (NASA). The NASA DC-8 aircraft platform sampled trace gas and aerosol concentrations through four scientific flights over California on 18, 20, 2, and 24 June 2008 and the flight paths are shown together in Fig. 2b. This mission had multiple scientific objectives, including improving the state emission inventories, characterizing off-shore shipping emissions, and quantifying the import of

Title Page

Abstract | Introduction

Conclusions | References

Tables | Figures

⏮ | ⏭

◀ | ▶

Back | Close

Full Screen / Esc

Printer-friendly Version

Interactive Discussion

pollution from Asia (Jacob et al., 2010). Ozone was measured by the NCAR team using the Chemiluminescence method. Two SO_2 measurement teams (CIT and GIT) and two SO_4 measurement teams (UNH and CU – Boulder) were on board for all the flights (http://www-air.larc.nasa.gov/cgi-bin/arcstat-c). The CIT and GIT teams both used

5   chemical ionization mass spectroscopy (CIMS), and UNH and CU-Boulder (CUB) used Soluble Acidic Gases and Aerosol (SAGA) and Aerosol Mass Spectrometry (AMS), respectively (Weinheimer et al., 1994; Scheuer et al., 2003; McNaughton et al., 2007; Slusher et al., 2004; Crounse et al., 2009; Dunlea et al, 2009). These data were averaged every one minute for use in this study.

10   In addition to the airborne measurements, surface measurements were analyzed. The data analyzed included continuous hourly SO_2 measurements with low instrument sensitivity from CARB surface sites (http://www.arb.ca.gov/qaweb/siteinfo.php), EPA Air Quality System (AQS) daily-averaged fine PM (diameter 0–2.5 µm) speciation data (including SO_4) at a variety of California urban sites on 20 and 23 June (http://www.epa.

15 gov/ttn/airs/airsaqs/detaildata/downloadaqsdata.htm), daily-averaged fine SO_4 mass from Interagency Monitoring of Protected Visual Environments (IMPROVE) sites on 20 and 23 June (http://views.cira.colostate.edu/web/DataWizard/), and weekly-averaged SO_4 mass at six Californian Clean Air Status and Trends Network (CASTNET) surface sites over the remote areas.

20 2.2   Model, meteorology and boundary conditions

We simulated the ARCTAS – CARB period (18–24 June) using the Sulfur Transport and dEposition Model (STEM) – Version 2K3. The modeling system applied here included three components, a hemisphere tracer model in 60 km grids; a continental scale gas-phase and aerosol chemical transport simulation in 60 km grids, and a regional-scale

25 gas-phase and aerosol chemical transport domain centered over California in 12 km grids. Meteorology fields for all three grids were generated by the Advanced Research Weather Research & Forecasting Model (WRF-ARW) Version 2.2.1 (Skamarock et al., 2007) with forecast and reanalyzed meteorological inputs (Mesinger et al., 2006) for the

Ozone and sulfur oxides levels over California

M. Huang et al.

Full Screen / Esc

Printer-friendly Version

Interactive Discussion

60 km and 12 km simulations, respectively. Different boundary conditions were used in this study for the 60 km and 12 km simulations. In the 60 km base case, lateral boundary conditions (LBC) for thirty gaseous species and top boundary conditions for ten gaseous species were obtained from the archived RAQMS global model predictions. The LBCs for several aerosols (BC, OC, dust, sea salt and SO_4) were taken from the 60 km STEM tracer results. The details of model configuration are described in Huang et al. (2010) and Table 1.

2.3 Emissions

Emission inputs for each of the three modeling components differed slightly, based on respective demands for resolution and completeness. In the hemispheric tracer model, we used a bottom-up global gridded inventory developed for the ARCTAS mission (Streets et al., 2008, http://mic.greenresource.cn/arctas_premission). This inventory is driven by regional-specific information on fuels and activity from various economic sectors, including anthropogenic, biomass and global shipping. In the 60 km continental model, anthropogenic emissions for North America were taken from the 2001 National Emissions Estimate Version 3 (NEI 2001), an update of the 1999 US National Emissions Inventory with growth factors applied by Source Classification Code, and augmented with national inventories for Canada (2000) and Mexico (1999). The NEI 2001 includes emission around the port area, but misses the shipping emissions over the ocean. Daily biomass burning emissions from the Real-time Air Quality Modeling System (RAQMS) (Pierce et al., 2007) were provided by the Cooperative Institute for Meteorological Satellite Studies (CIMSS). Biogenic emissions of monoterpene and isoprene were taken from twelve-year-averaged values from the Orchidee model (Lathiere et al., 2006). For the 12 km model the anthropogenic and biogenic emissions were re-gridded from a contemporary CARB 4 km emission inventory. The anthropogenic emissions outside of the CARB domain (including Mexico, states of Nevada, Washington and Idaho) were also taken from NEI 2001, same as in the 60 km base simulation. Biomass burning emissions were generated by the prep-chem-source model

(WRF/Chem Version 3.1 users' guide, 2009), which used MODIS – detected point fire information at 1 km ground resolution (Giglio et al., 2003; Davies et al., 2009) and was adjusted at each time step to match total emissions rates from RAQMS. H_2S and DMS emissions were not included in these cases.

3 Results and discussions

3.1 General conditions and O_3 levels in base cases

The California summer climate in 2008 was hot and dry, influenced by the Pacific high pressure system. Wildfire events broke out on 21 June at various locations over both northern and southern California. On 18–20 June, fires were detected along the California-Mexico border.

The 12 km average WRF-modeled 10 m winds at multiple times (00:00, 06:00, 12:00 and 18:00 UTC) over California during the experiment week are shown in Fig. 1. The northwesterly winds along the coast and through the central valley, together with the sea-land breezes, determined the regional transport of pollutants. The wind vectors are colored with predicted mixing layer height (PBLH). The PBLH over the ocean stayed below 500 m, while the PBLH over the SC terrestrial areas reached up to ~1500 m during daytime. These are consistent with vertical structures of short-lived chemicals from the aircraft measurements.

During the ARCTAS-CARB period, the DC-8 flight collected air-samples over coastal areas and the Central Valley, including three regions with relatively high population and high pollution levels – South Coast (SC), San Francisco Bay area (SF), and Fresno in the Central Valley (CV). We focus this study on the SC area because it had the largest number of flight-collected air samples, although analysis was also done over the SF and CV area. The SC, SF and CV domains are defined in boxes in Fig. 2b. The latitude/longitude ranges that the three regions cover are 33° N–34.5° N, 121° W–117° W; 37° N–39° N, 123° W–121° W; 36° N–37° N, 119° W–121° W, respectively.

The four DC-8 flight paths are also shown in Fig. 2b. Three (18, 22, 24 June) out of the four flights took measurements over the SC area during approximately 15:00–24:00 UTC (08:00 a.m.–05:00 p.m. LT). All of observed O_3 concentrations along these flights below ~1000 m are shown in Figs. 2a and 3b horizontally and vertically, respectively. Observed O_3 ranged from less than 40 ppb to ~120 ppb, and with little vertical structure. The highest O_3 levels (>120 ppb) were found around Riverside. The O_3 levels over the ocean were below 80 ppb.

The modeled O_3 concentrations from the two resolutions are shown in Fig. 3a, for the flight time average O_3, and for the averaged daily maximum O_3. Results from both simulations predicted O_3 concentrations over the Central Valley over 70 ppb, and the 12 km predicted ~5 ppb higher O_3 over southern California during the flight times. The 12 km results show lower average O_3 levels over northern California, southern California urban areas, and more fine-scale features than the 60 km results. The predicted average daily maximum O_3 levels from 12 km and 60 km simulations occur in similar regions in the Central Valley and a large part of the southern California, but the 12 km case predicted higher values (>100 ppb) than the 60 km case (80–90 ppb).

Figure 3b compares the predicted O_3 for the two model resolutions with all flight observations below 1000 m vertically. The 12 km simulations predict higher concentrations, show stronger variations and higher correlation with the flight observations – R (12 km) and R (60 km) are 0.62 and 0.58, respectively.

Within the SC domain, six CARB surface sites that measure O_3 and SO_2 hourly concentrations were selected for this study. Their locations are illustrated in Fig. 2c, and Fig. 3c compares the average (six sites) observed and modeled O_3 time series at these sites. The 12 km simulations indicate the stronger diurnal variations and higher correlations with observations – R (12 km) and R (60 km) are 0.73 and 0.6, respectively.

3.2 Influences of natural source emissions on SC O_3

In order to quantify the impacts of natural emission sources on SC O_3 levels, we conducted two sensitivity simulations in the 12 km grids. We turned off the biogenic

Ozone and sulfur oxides levels over California

M. Huang et al.

(isoprene and monoterpene) emissions and wildfire emissions for the two cases, respectively, and analyzed the changes of O_3 between the base and each of the sensitivity cases. Thus these studies are designed to look at the contribution of natural sources within CA to CA surface O_3 levels, and differ from previous studies that have looked largely at the impact of natural sources globally. As O_3 formation is non-linear, the differences between base and sensitivity cases contain some uncertainties, but provide practical suggestions for regulations.

Figure 4a shows the 24-h average isoprene and monoterpene emissions from the CARB EI. Their emissions are highly related to the land use type (not shown) and vary over California. Isoprene and monoterpene emission rates are the highest over northern California regions covered by evergreens, and account for 40%–60% of total NMVOC emissions over those regions. In contrast, in the Central Valley and south coast urban areas, the emission rates are more than 20 times lower, accounting for less than 2% of the total NMVOC emissions (not shown).

The differences of flight time and daily maximum surface O_3 during the flight week between the base and no-biogenic emission cases are shown in Fig. 4c, and e, respectively. The largest O_3 decrease is found over northern California and the CV, with the flight time O_3 changes up to 6 ppb and the average daily maximum changes ranging from 6–12 ppb. In contrast, the O_3 changes over the SC area stay between 2–4 ppb.

The differences of 24-h average surface CO during the flight week between the base and no-fire emission cases are shown in Fig. 4b. Analysis of the impacts from wildfires in North Asia and Europe, and South Asia and Africa using the tracer model indicate that the fires that occurred outside of the North America had negligible impacts on surface SC air quality (<5% below ∼1.5 km, not shown).

The highest differences (>100 ppb) due to California fires occur over northern California, where the wildfires were most intense and durations the longest. Fire locations with changes in CO of 400–800 ppb are shown in northern California and the Monterey Bay areas, and the fire impacts on CO extend to the SC coastal areas (20–50 ppb of delta CO). The differences of flight time and daily maximum surface O_3 during the flight

week between the base and no-fire emission cases are shown in Fig. 4d and f, respectively. The largest changes in averaged daily maximum O_3 occur over the northern part of California-Nevada border, at 9–15 ppb. Negative O_3 changes can be found around the fire locations, indicating the strong influences of aerosol emissions from fires. Over the SC area, the fire impacts on the average surface maximum and flight time O_3 stay below 2–3 ppb.

To better understand the impact of biogenic and fire emissions on O_3 concentrations within the boundary layer, we calculate the model sensitivity with Eq. (1) each of the one-minute flight data below 1000 m.

$$\text{Sensitivity (\%)} = \frac{\left|\text{base case } O_3 - \text{sensitivity case } O_3\right|}{\text{base case } O_3} \cdot 100\% \tag{1}$$

The model sensitivities are plotted in Fig. 5a and b. The sensitivities in both cases are below ∼30%. Both resolutions show that the O_3 over CV area was largely affected by biogenic emissions. The O_3 over northern CV, the SF coast, and the central coast were highly impacted by the fire emissions.

The mean and maximum sensitivity for each flight day in SC are summarized in Table 2. The mean 12 km model results show that biogenic and fire emissions contributed 2.3% and 4.3%, respectively, to near surface O_3 over SC (with maximum values reaching contributions of 8.9% and 26.6% for each of these sources, respectively). The contributions of biogenic and fire emissions were even higher in regions outside of SC.

To help assess the uncertainties in estimating the role of natural emissions, no-biogenic and no-fire emission sensitivity simulations were also conducted in the 60 km grid domain. The 24-h average Orchidee EI (Fig. 6a) shows a smoother but similar spatial pattern as the 12 km CARB estimates, with the maximum emission rates over northern California, lower than the CARB EI. Moreover, the magnitudes are much lower than the CARB EI along the coastal areas and higher over southeastern California. Delta O_3 between the 60 km base and no-biogenic emission cases are shown in Fig. 6c and e. The changes in average daily maximum O_3 are of similar magnitude as in the

Ozone and sulfur oxides levels over California

M. Huang et al.

Title Page

Abstract | Introduction

Conclusions | References

Tables | Figures

|◄ | ►|

◄ | ►

Back | Close

Full Screen / Esc

Printer-friendly Version

Interactive Discussion

12 km grids over northern California and CV, but are 5–8 ppb over the SC area, higher than the changes in 12 km grids. The O_3 changes during flight time also differ from the 12 km cases, with higher magnitudes overall (changes over the SC of 5–6 ppb). The different O_3 changes over SC between the two resolution cases are not only due to the emission differences within California, but also reflect the impacts of model resolution on flow fields, mixing layer height, and the contributions from the Nevada and Mexico biogenic emissions which the CARB EI does not include.

The differences of daily maximum surface O_3 during the flight week between the base and no-fire emission cases in 60 km grids are shown in Fig. 6f. Same as in the 12 km cases, the highest changes occur over the north part of California-Nevada border (9–15 ppb). Figure 6d shows higher flight time average O_3 changes than in the 12 km cases (approximately doubled magnitudes over most areas). Negative O_3 changes are not found over California because the coarse resolutions smooth the intensity of fire emissions, as the CO differences in Fig. 6b show. Over the SC area, the fire impacts on the average surface maximum and flight time O_3 stay below ∼3–4 ppb.

The model sensitivity along all SC flight paths below 1000 m in 60 km grids are shown in Fig. 5c, d and Table 2. The 60 km simulations show high sensitivity of O_3 to biogenic emissions along the southern California-Mexico border. Due to the Mexico biogenic emissions, the 60 km differences between base and no-biogenic emissions cases are higher at SC. Stronger model sensitivity to fire emissions is found over that region and less strong sensitivity to fire emissions can be seen along the coastal SC areas, indicating the effects of model resolution and fire locations.

The sensitivity studies conducted in two resolutions suggest that fire and biogenic emissions play more important roles in O_3 production over areas out of SC during the ARCTAS-CARB period. The different model configurations indicate a 3–4 ppb uncertainty due to various factors (such as resolution, EIs, meteorology fields).

3.3 SO$_x$ spatial distributions and model-observation comparisons

The model-predicted 24-h surface average total sulfur levels during the experiment week from the two different model resolutions are shown in Fig. 7a–b. The corresponding SO$_2$ contributions to total sulfur (SO$_2$+SO$_4$, SO$_4$ was converted to ppb) are also
5 shown in Fig. 7c–d. Elevated sulfur levels can be seen over SC, SF and Fresno in CV, as well as around the California – Nevada border and the west California – Mexico border, due to the fresh emissions (SO$_2$ %>60%). The sulfur levels at these areas from the 60 km simulations are generally lower than the 12 km case, especially over the SC area. Due to the lack of the shipping emissions in the NEI 2001, the sulfur levels over
10 the ocean are low in the 60 km case, except the near-shore areas of the central coast. In contrast, the 12 km base case shows more detailed local features over land and the gradients along ship tracks in the ocean.

Figure 7e, f shows the observed total sulfur along all DC-8 flights (below 1 km a.s.l.), together with the SO$_2$ % in the SC area. The observed total sulfur is the sum of
15 averaged SO$_2$ and SO$_4$ (units are converted to ppb) measured by different teams. The SO$_2$ % is the ratio of the averaged SO$_2$ concentrations measured by the two teams over the total sulfur concentrations. Similar to the model simulations, fresh SO$_2$ (SO$_2$ %>60%) and higher sulfur levels were observed within the three regions. Over SC, SO$_x$ levels were higher at on-shore port areas, such as around Long Beach (up to
20 6–12 ppb), than over the inland areas (below ~1–2 ppb).

The modeled total sulfur concentrations are compared with observations along all SC DC-8 flights (below 5 km a.s.l.), and are shown as vertical profiles (averaged every 500 m) in Fig. 7i. The vertical structures constructed by binning data every 500 m and averaging them, show that sulfur was enhanced from the surface to ~3–4 km.
25 The observed average surface sulfur over this region was ~1.8 ppb below 500 m. The predictions show the lowest sulfur (and the highest biases) in the 60 km base case. The 12 km base case under-predicted total sulfur at all altitudes, but were improved over the 60 km base predictions.

Title Page

Abstract | Introduction

Conclusions | References

Tables | Figures

◀ | ▶

◀ | ▶

Back | Close

Full Screen / Esc

Printer-friendly Version

Interactive Discussion

The comparisons of observed and modeled SO_2 and SO_4 along all DC-8 flight paths over the three regions are also shown as vertical profiles in Fig. 7g, h. The GIT SO_2 is lower than the CIT SO_2 below 1 km and higher at ~1–3 km. The two sets of measured SO_4 follow the same trend below ~1.5 km, but CU Boulder SO_4 is ~10–20% lower than the UNH SO_4, and both teams observed SO_4 aloft at 2–4 km. The 60 km base case predicted the lowest SO_2 and SO_4. The 12 km base case SO_2 generally followed the CIT SO_2, but was biased low by ~50% at the surface. The general vertical structure of SO_4 was captured, but was more than 50% under-predicted at most altitudes.

The comparisons of observed and modeled SO_2 and SO_4 along all DC-8 flight paths are summarized in Table 3. The R values between modeled and observed SO_x, the Mean Biases (MB) as well as Root Mean Square Error (RMSE) of modeled SO_2 and SO_4 are listed. The higher correlations and lower errors are in bold. The 60 km base case predicted lower SO_2 and SO_4, and showed the weaker correlations with the observations. The 12 km base case improved the modeled SO_2 and SO_4 in magnitudes and correlations. As the partitioning between SO_2 and SO_4 is highly dependent on OH we also compared predicted OH and found that the 12 km base case had higher correlation than the 60 km case (0.47 compared to 0.41, respectively).

In addition to the comparisons of modeled SO_x along the DC-8 flight tracks, we also compare the predicted SO_2 and SO_4 with surfaces sites. Figure 8a shows the averaged of the daily average SO_2 at six SC surface sites (Fig. 3c). The 60 km base case under-predicted SO_2 more than 10 times in general. The 12 km base case produce higher maximum, minimum (not shown) and mean SO_2 values, and are closer to the observations.

Fine aerosol SO_4 (diameter 0–2.5 μm) mass was measured at multiple AQS-STN ground sites over California on 20 and 23 June, and at IMPROVE sites on the same days. These sites represent the fine SO_4 distributions over the urban and rural areas, respectively. In addition, the total SO_4 mass was measured and analyzed once a week at six California CASTNET sites, which are located at remote areas. There are several AQS-STN and IMPROVE sites located in SC domain, as Fig. 8c shows. No CASTNET

sites are located in the SC domain.

These observations are compared with results from both 12 km and 60 km simulations in Fig. 8b. The predictions from both cases are biased low by about a factor of two to three. The 12 km case results are improved over the 60 km predictions by more than a factor of two at the CASTNET and IMPROVE sites statewide and within SC.

From both modeled and observed SO_4 masses, it is found that during the flight week the surface values varied spatially according to: urban (AQS-STN) > rural (IMPROVE) > remote (CASTNET) areas, and the SC urban areas had higher fine SO_4 than the statewide average, while at SC rural areas the fine-mode SO_4 was lower.

In general, the 12 km results provide closer results to both flight and surface observations during the simulation week. We calculated the ratios of averaged observations over 12 km results along the flight paths and at surface sites in SC (Table 4). In general, the 12 km simulations underestimated SO_2 by up to $\sim$1.8 times and SO_4 by more than 2.5 times. During the flight periods, the ratios of the under-prediction along flight paths and at six surface sites were similar (1.71 and 1.79, respectively). These ratios will be used to scale the 12 km results in Sect. 3.7. The scaling factors calculated along flight paths and surface sites represent the daytime (15:00–24:00 UTC, 10 h) and 24 h conditions. We further derived the scaling factors during nighttime using:

$$\text{factors (24 hours)} = \frac{\text{factors (flight time)} \cdot 10 + \text{factors (night time)} \cdot 14}{24} \tag{2}$$

These night time scaling factors are also given in Table 4.

3.4 The identification of the contributors to the elevated SO_x concentrations

Figure 7g–i shows that SO_x was elevated along the SC flight tracks near surface and between 2–4 km. To better understand the possible source contributors to the elevated SO_x levels near the surface, we summarize the VOC age and CO contributions in Table 5 for flight segments below 1 km using the tracer calculations. During the experiment week, most of the air-masses had China CO % contributions less than 0.5%

and North America CO %>99%, except the air-masses on 24 June during UTC 23:00–24:00 (during flight) that had China CO % of ~40%. These air-masses are described in detail in Sect. 3.5.

In order to identify the air-mass sources that caused the elevated sulfur aloft over SC between 2–4 km (Fig. 7g–i), we analyzed back-trajectories originating along the three SC DC-8 flight paths at 2–4 km a.s.l. on individual flight days, based on the 12 km meteorological fields. During the flights on 18 and 24 June, the air was lifted and moved from the Central Valley. In contrast, during the other flight day, air masses were from the southwest, and they descended from >3500 m to SC (not shown in figures).

3.5 Long-range transport events

Long-range transport of pollutants from Asia is typically assumed to be weaker and less frequent during summertime relative to springtime. During the ARCTAS-CARB experiment week, the 22 June flight aimed at characterizing the upwind boundary conditions necessary to model inland O_3 and aerosols (Jacob et al., 2010). On this day, the DC-8 took off from Palmdale, CA, flew over the Pacific Ocean to THD, and then circled back to Palmdale along the coast (Fig. 2b). At the outbound part of this flight (approximating UTC 17:00–21:00 UTC), strong Asian inflows were encountered, as indicated from the VOC age (ranging from 200–400 h) shown in Fig. 9a, together with the five – day back trajectories based on the 60 km WRF meteorology fields in Fig. 9e. Vertical profiles and time series of observed and modeled SO_2 and SO_4 are shown in Fig. 9a–d for this flight. Elevated SO_4 was observed at 6–8 km (up to ~6 µg/sm^3) a.s.l., mainly at flight leg 2 and partially at leg 3, by the CUB team. These air-masses were also high in China CO % based on the tracer model calculations (not shown) at 6–8 km (Fig. 9a). Three – day forward trajectories originating from >6 km a.s.l. flight heights based on the 12 km WRF meteorology fields are shown in Fig. 9f, and as shown the air-masses at these heights generally traveled above 3 km a.g.l. over California and thus did not impact the CA surface concentrations.

Ozone and sulfur oxides levels over California

M. Huang et al.

At flight leg 3 (THD), the DC-8 also observed slightly enhanced SO_4 at 1–4 km (Fig. 9a). In a previous study, we concluded that elevated O_3 levels at 2–4 km on the same flight day in the eastern Pacific can be transported into the northern central valley, affecting several surface sites there. These air-masses are also transported further into southern California (Fig. 9g). We estimate that these air masses contributed $\sim$0.5 μg/sm^3 to near-surface SO_4 levels over SC on 24 June, as summarized in Table 5. The enhancements of SO_4 by foreign air-masses along the SC flight paths are calculated by Eq. (3)

Enhancements = (1 – North America CO %)·average SO_x by two teams   (3)

SO_2 peaks (<0.7 ppb) were also observed by the CIT team at 6–8 km a.s.l. at flight legs 1 and 2. These were the residuals in Asian plumes, as indicated by similar peaks for a number of observed species and the tracer calculations (not shown). The RAQMS and the 60 km base case used as boundary conditions missed the SO_2 peaks at both legs 1 and 2, but as discussed for SO_4, these air-masses containing high SO_2 did not affect California surface air quality. Only $\sim$0.1 ppb of near-surface SO_2 was attributed to foreign sources (Table 5), and the boundary conditions captured SO_2 levels at 2–4 km very well between 1.5–4 km (Fig. 9b).

3.6 SO_x local emissions – emission inventory comparisons

As the local emissions mainly contributed to the elevated SO_x concentrations near the surface during the experiment period, it is important to understand the contributions of the local sources. Therefore the emission inventory is one of the most important model inputs affecting the model- simulated near-surface SO_x concentrations.

Figure 10 compares the 24-h average surface SO_x emissions during 18–24 June from the CARB EI and NEI 2001 EI simulations (12 km and 60 km cases) over SC. Shipping emissions are included in the CARB EI while not in the NEI 2001, and the terrestrial SO_2 emissions in NEI 2001 are generally much lower as shown in Fig. 10a, b. Figure 10c compares the time series of the average emission rates over the six

SC surface sites from both EIs. The CARB EI peaks around noon time while the NEI shows sharper later afternoon peaks (pm rush hours). The magnitudes in CARB emission rates are much higher than NEI, ~12 times for the 24 h averaged emission rates at the six sites (6×10^{10} and 5×10^{9} molecules/cm^2/s, respectively).

Table 6 quantifies the mean and maximum surface SO_x emission rates in SC and the entire state from both EIs. The statewide mean and maximum emission rates from NEI are higher than the CARB EI. However, in SC, the situation is opposite. The biggest SO_x emission sources in SC and California in NEI and CARB EI also differs. In the CARB EI, the shipping emissions account for 52.1% and 44.6% of summertime SO_x emissions for SC and the entire state, while in NEI, fossil fuel combustion and non-road equipment rank as the top emission sources in LA county and California, respectively.

3.7 Effects of maritime SO_x emissions on coastal SC air quality

As analyzed in Sect. 3.6, shipping emissions over the SC (and other California coastal areas) account for more than 40–50% of total summertime SO_x emissions. Therefore, the SO_x levels at SC are contributed by both terrestrial (highway, port heavy transportations, industry) and maritime emissions (shipping). As for the important O_3 precursors, the shipping emissions account for ~19% and 14.5% of the total NO_x emissions in SC and the state, while VOC emissions from ships are negligible.

To further understand the contributions from terrestrial and maritime emissions to sulfur and O_3 concentrations over SC, we conducted an additional model simulation in 12 km with only the terrestrial emissions from the CARB EI for all chemical species. The differences between the base case and the terrestrial-emission-only case provide an estimate of the contribution from shipping.

The 24-h averaged SO_2 and fine SO_4 from the 12 km base case and the contributions from maritime sulfur emissions during the flight week are shown in Fig. 11. The spatial distributions have been scaled by multiplying flight time and night time scaling factors (Table 4) for SO_2 and SO_4, respectively, in order to correct the uncertainties imported from the original CARB EI. SO_2 concentrations are directly affected by both terrestrial

and maritime emissions as shown. As expected, the terrestrial emissions lead to high SO_2 concentrations over land and on shore, and the maritime emissions cause high SO_2 levels over the ocean and on shore (where $SO_2 > 60-70\%$ of the total sulfur). The contributions to inland SO_2 levels are much lower (0.2–0.5 ppb, also shown in Fig. 8a at six SC surface sites). For SO_4, the spatial distribution is highly influenced by reaction rate and the wind fields. SC is heavily under the impact of northwest winds during the daytime. Consequently, the maritime emissions generally contributed 30–50% of SO_4 along the coast (1.5–2.5 µg/m^3) and further affected extended areas on land by 20–30% of SO_4 (0.5–1 µg/m^3). This effect extends as far as San Diego and the California – Mexico border area.

Figure 7g–i shows the change of the vertical distributions of SO_x in response to cutting off maritime emissions along all SC DC-8 flight paths (Labeled as case TR in the Figures). During the flight periods, both SO_2 and SO_4 were reduced in the vertical up to ~1500 m. The maximum reduction of SO_x is shown at the lowest 500 m, by ~50%. The differences in simulated SO_2 in 12 km base and terrestrial emission cases are ~0.3–0.5 ppb for each day during the week at the six surface sites (Fig. 8a, even though daily variations on SO_2 are high).

The effects of maritime emissions on surface O_3 levels are shown in Fig. 12. The flight time average O_3 changes for the flight week are below 3 ppb, and over the port areas (such as north Long Beach, the flight time average O_3 increases by 3–4 ppb after cutting off the maritime emissions. The averaged daily maximum O_3 decrease by 3–7 ppb in the domain, and the decrease around north Long Beach are lower (~3–4 ppb). Figure 12e shows the daily flight time O_3 observations and the predictions from 12 km and 60 km base cases, together with O_3 from the terrestrial emission case for the six SC surface sites. The differences in simulated O_3 in the 12 km base and terrestrial emission cases are below 5 ppb for each day.

To better understand the reduction of SC O_3 caused by maritime emissions, the changes of two O_3 production indicator species (NO_y and O_3/NO_y) are analyzed in Fig. 13. When $NO_y < 10-25$ ppb, or/and $O_3/NO_y > 5-10$, the area belongs to the NO_x-

limited ozone production regime (Milford et al., 1994; Sillman et al., 1995; Jacob et al., 1995). Based on these criteria, the SC urban area in the 12 km base case is VOC limited. The removal of maritime emissions leads to flight time average NO_y decreases up to 14–16 ppb, over the North Long Beach area, and the O_3/NO_y ratio rises to 5–10. This indicates that by cutting off the maritime emissions, some coastal areas such as North Long Beach can change from VOC-limited to NO_x-limited.

4   Conclusions

The chronic O_3 problems as well as the increasing SO_x ambient concentrations over California's south coast (SC) and other regions are affected by both long-range transport and local emissions. Asian inflows were shown to be important around June 22, when the O_3 concentrations in long-range transported air were 60–80 ppb (Huang et al., 2010). The transported air at ~2–4 km contained ~0.6–0.7 µg/sm^3 of SO_4 in average that descended to the surface and influenced surface concentrations. The contribution from long-range transport occurred first over northern California and then over SC through in-state transport on ~24 June, when up to 0.5 µg/sm^3 of surface SO_4 in SC was attributed to foreign sources. During this period SO_4 and SO_2 in these long-range transported air-masses were also enhanced at altitudes above 6 km, but were transported at inland at high altitudes and did not influence CA surface air quality.

The influence of local emissions from both natural and anthropogenic sources on air quality was evaluated. We conducted sensitivity simulations by turning off biogenic and fire emissions in both 12 km and 60 km model resolutions and compared the modeled O_3 in base vs. sensitivity cases. We found that both biomass burning and biogenic emissions contribute to regional background O_3 over SC up to 4 ppb, with larger contributions in other regions of CA (such as in the Central Valley, up to 10–12 and 12–15 ppb from biogenic and fire emissions, respectively). Uncertainties in these estimates due to model resolutions and emissions inventories are on the order of 3–4 ppb over SC.

The high concentrations of SC surface SO_x during the flight week were mostly contributed by local emissions. We compared two anthropogenic SO_x EIs applied in 60 km and 12 km simulations and evaluated the model performance. The EIs vary temporally and spatially, but the NEI 2001 lacks the shipping emissions, and has lower emissions overall. The CARB 2005 EI improved the magnitudes of emission rates and produced results closer to observations. However, the overall SO_x emissions over the SC are shown still to be underestimated, and estimate that 2008 emissions are low by about factor of two.

We also analyzed the effects of maritime emissions on O_3 and SO_x distributions over SC by conducting a sensitivity simulation without maritime emissions using the CARB EI. The maritime emissions contributed up to 5 ppb to SO_2 concentrations over the ocean and on-shore area. Fine SO_4 along the downwind areas increased by 0.2–2 µg/m^3 due to the maritime emissions. The maritime emissions significantly increased the NO_y distributions on shore especially around the port area of North Long Beach and changed this area from VOC-limited to NO_x-limited after cutting off maritime emissions. The impacts of maritime emissions on flight time and average daily maximum O_3 levels over this area are different from over the surrounding areas.

A similar analysis for SO_x was done over the SF and CV regions (Fig. 2b) and we suggest further improvement on EIs over these regions. In general, by using the CARB EI, the model underestimated SO_x concentrations by a factor of up to 2 at SF and more than 10 times around Fresno areas, and the NEI leads to much lower predictions. Fewer observational data are available for these areas than SC during the flight week, causing inconsistency of the underestimation extents along flight paths and at the surface, and further studies are needed.

Ozone and sulfur oxides levels over California

M. Huang et al.

Title Page

Abstract	Introduction
Conclusions	References
Tables	Figures

◄ | ►►

◄ | ►

Back | Close

Full Screen / Esc

Printer-friendly Version

Interactive Discussion

References

BST Associates: Trade impacts study Prepared for Port of Los Angeles, Port of Long Beach, available at: http://www.portoflosangeles.org/DOC/REPORT_ACTA_Trade_Impact_Study.pdf, 2007.

Bytnerowicz, A., Cayan, D., Riggan, P., Schilling, S., Dawson, P., Tyree, M., Wolden, L., Tissell, R., and Preisler, H.: Analysis of the effects of combustion emissions and Santa Ana winds on ambient ozone during the October 2007 southern California wildfires, Atmos. Environ., 44, 678–687, 2010.

Corbett, J. J. and Fischbeck, P. S.: Emissions from ships, Science, 278, 823–824, 1997.

Cox, P., Delao, A., Komorniczak, A., and Weller, R.: The California almanac of emissions and air quality 2009 edition, available at: http://www.arb.ca.gov/aqd/almanac/almanac09/almanac2009all.pdf, 2009.

Crounse, J. D., DeCarlo, P. F., Blake, D. R., Emmons, L. K., Campos, T. L., Apel, E. C., Clarke, A. D., Weinheimer, A. J., McCabe, D. C., Yokelson, R. J., Jimenez, J. L., and Wennberg, P. O.: Biomass burning and urban air pollution over the Central Mexican Plateau, Atmos. Chem. Phys., 9, 4929–4944, doi:10.5194/acp-9-4929-2009, 2009.

Davies, D. K., Ilavajhala, S., Wong, M.M., and Justice, C.O.: Fire Information for Resource Management System: Archiving and Distributing MODIS Active Fire Data, IEEE T. Geosci. Remote, 47(1), 72–79, 2009.

Dunlea, E. J., DeCarlo, P. F., Aiken, A. C., Kimmel, J. R., Peltier, R. E., Weber, R. J., Tomlinson, J., Collins, D. R., Shinozuka, Y., McNaughton, C. S., Howell, S. G., Clarke, A. D., Emmons, L. K., Apel, E. C., Pfister, G. G., van Donkelaar, A., Martin, R. V., Millet, D. B., Heald, C. L., and Jimenez, J. L.: Evolution of Asian aerosols during transpacific transport in INTEX-B, Atmos. Chem. Phys., 9, 7257–7287, doi:10.5194/acp-9-7257-2009, 2009.

Ozone and sulfur oxides levels over California

M. Huang et al.

Title Page

Abstract	Introduction
Conclusions	References
Tables	Figures

|◄ | ►|

◄ | ►

Back | Close

Full Screen / Esc

Printer-friendly Version

Interactive Discussion

Fiore, A., Jacob, D. J., Liu, H., Yantosca, R. M., Fairlie, T. D., and Li, Q.: Variability in surface ozone background over the United States: Implications for air quality policy, J. Geophys. Res., 108(D24), 4787, doi:10.1029/2003JD003855, 2003.

Giglio, L., Descloitres, J., Justice, C. O., and Kaufman, Y. J.: An Enhanced Contextual Fire Detection Algorithm for MODIS, Remote Sens. Environ., 87, 273–282, 2003.

Huang, M., Carmichael, G. R., Adhikary, B., Spak, S. N., Kulkarni, S., Cheng, Y. F., Wei, C., Tang, Y., Parrish, D. D., Oltmans, S. J., D'Allura, A., Kaduwela, A., Cai, C., Weinheimer, A. J., Wong, M., Pierce, R. B., Al-Saadi, J. A., Streets, D. G., and Zhang, Q.: Impacts of transported background ozone on California air quality during the ARCTAS-CARB period – a multi-scale modeling study, Atmos. Chem. Phys., 10, 6947–6968, doi:10.5194/acp-10-6947-2010, 2010.

IPCC: Contribution of Working Group I to the Fourth Assessment Report of the Intergovernmental Panel on Climate Change, Climate Change 2007: The Physical Science Basis, Cambridge, United Kingdom and New York, NY, USA, Cambridge University Press, 2007.

Jacob, D. J., Horowitz, L. W., Munger, J. W., Heikes, B. G., Dickerson, R. R., Artz, R. S., and Keene, W. C.: Seasonal transition from NO_x to hydrocarbon-limited conditions for ozone production over the eastern United States in September, J. Geophys. Res., 100, 9315–9324, 1995.

Jacob, D. J., Crawford, J. H., Maring, H., Clarke, A. D., Dibb, J. E., Emmons, L. K., Ferrare, R. A., Hostetler, C. A., Russell, P. B., Singh, H. B., Thompson, A. M., Shaw, G. E., McCauley, E., Pederson, J. R., and Fisher, J. A.: The Arctic Research of the Composition of the Troposphere from Aircraft and Satellites (ARCTAS) mission: design, execution, and first results, Atmos. Chem. Phys., 10, 5191–5212, doi:10.5194/acp-10-5191-2010, 2010.

Koo, B., Chien, C.-Y., Tonnesen, G., Morris, R., Johnson, J. Sakulyanontvittaya, T., Piyachaturawat, P., and Yarwood, G.: Natural emissions for regional modeling of background ozone and particulate matter and impacts on emissions control strategies, Atmos. Environ., 44, 2372–2382, 2010.

Lathière, J., Hauglustaine, D. A., Friend, A. D., De Noblet-Ducoudré, N., Viovy, N., and Folberth, G. A.: Impact of climate variability and land use changes on global biogenic volatile organic compound emissions, Atmos. Chem. Phys., 6, 2129–2146, doi:10.5194/acp-6-2129-2006, 2006.

McNaughton, C. S., Thornhill, L., Clarke, A. D., Howell, S. G., Pinkerton, M., Anderson, B., Winstead, E., Hudgins, C., Maring, H., Dibb, J. E., and Scheuer, E.: Results from the DC-

inlet characterization experiment (DICE): Airborne versus surface sampling of mineral dust and sea salt aerosols, Aerosol Sci.Technol., 40, 136–159, 2007.

Mesingera, F., DiMego, G., Kalnay, E., Mitchell, K., Shafran, P. C., Ebisuzaki, W., Jovic, D., Woollen, J., Rogers, E., Berbery, E. H., Ek, M. B., Fan, Y., Grumbine, R., Higgins, W., Li, H., Lin, Y., Manikin, G., Parrish, D., and Shi, W.: North American Regional Reanalysis, B. Am. Meteor. Soc., 87(3), 343–360, doi:10.1175/BAMS-87-3-343, 2006.

Milford, J. B., Gao, D., Sillman, S., Blossey, P., and Russell, A. G.: Total reactive nitrogen (NO_y) as an indicator of the sensitivity of ozone to reductions in hydrocarbon and NO_x emissions, J. Geophys. Res., 99, 3533–3542, 1994.

NASA: OMI O_3 column data source: ftp://toms.gsfc.nasa.gov/pub/omi/data/ozone/Y2008/, 2008.

NCEP/NOAA: Real-time, global, sea surface temperature (RTG_SST) analysis data source: ftp://polar.ncep.noaa.gov/pub/history/sst/, 2008.

NOAA: 2010 CalNex Science and Implementation Plan, http://www.esrl.noaa.gov/csd/calnex/scienceplan.pdf, 2008.

Pfister, G. G., Wiedinmyer, C., and Emmons, L. K.: Impacts of the fall 2007 California wildfires on surface ozone: Integrating local observations with global model simulations, Geophys. Res. Lett., 35, L19814, doi:10.1029/2008GL034747, 2008.

Scheuer, E., Talbot, R. W., Dibb, J. E., Seid, G. K., deBell, L., and Lefer, G.: Seasonal distributions of fine aerosol sulfate in the North American Arctic Basin during TOPSE, J. Geophys. Res., 108, 8370, doi:10.1029/2001JD001364, 2003.

Sillman, S.: The use of NO_y, H_2O_2, and HNO_3 as indicators for ozone-NO_x-hydrocarbon sensitivity in urban locations, J. Geophys. Res., 100, 14175–14188, 1995.

Slusher, D. L., Huey, L. G., Tanner, D. J., Flocke, F. M., and Roberts, J. M.: A thermal dissociation-chemical ionization mass spectrometry (TD-CIMS) technique for the simultaneous measurement of peroxyacyl nitrates and dinitrogen pentoxide, J. Geophys. Res., 109, D19315, doi:10.1029/2004JD004670, 2004.

Viswanathan, S., Eria, L., Diunugala, N., Johnson, J., and McClean, C.: An analysis of effects of San Diego wildfire on ambient air quality, J. Air Waste Manag. Assoc., 56(1), 56–67, 2006.

Vutukuru, S. and Dabdub, D.: Modeling the effects of ship emissions on coastal air quality: A case study of southern California, Atmos. Environ., 42, 3751–3764, 2008.

Wang, H., Jacob, D. J., Sager, P. L., Streets, D. G., Park, R. J., Gilliland, A. B., and van Donkelaar, A.: Surface ozone background in the United States: Canadian and Mexican pollution

Ozone and sulfur oxides levels over California

M. Huang et al.

Title Page

Abstract	Introduction
Conclusions	References
Tables	Figures

|◄ | ►|

◄ | ►

Back | Close

Full Screen / Esc

Printer-friendly Version

Interactive Discussion

influences, Atmos. Environ., 43, 1310–1319, 2009.

Weinheimer, A. J., Walega, J. G., Ridley, B. A., Gary, B. L., Blake, D. R., Blake, N. J., Rowland, F. S., Sachse, G. W., Anderson, B. E., and Collins, J. E.: Meridional distributions of NOx, NO_y, and other species in the lower stratosphere and upper troposphere during AASE II, Geophys. Res. Lett., 21, 2583–2586, 1994.

WRF/Chem Version 3.1 User's Guide: http://ruc.noaa.gov/wrf/WG11/Users_guide.pdf, 2009.

Ozone and sulfur oxides levels over California

M. Huang et al.

Table 1. Summary of STEM inputs for base cases in two resolutions.

Inputs	Source Data		Resolutions	
	60 km/18 layers/6 h base case	12 km/32 layers/1 h base case	60 km	12 km
Meteorology, WRF 2.2.1	GFS + one time step SST	NARR + daily SST	6 h, 1°× 1°	3 h, 36 km
Ozone column, required by the TUV model	Measured by Ozone Mapping Spectrometer (OMI) instrument on board the NASA Aura spacecraft, daily		1°×1°, 1 day	
Anthropogenic Emissions (point and mobile)	NEI 2001, weekday varied from weekends	CARB 2005, projected from 2002, daily varied. Out of CARB domain filled with NEI 2001	1°× 1°, 1 h	4 km × 4 km, 1 h
Biogenic Emissions	Orchidee	CARB 2005 projected from 2002, daily varied	1°× 1°, monthly averaged	4 km × 4 km, 1 h
Biomass burning Emissions	RAQMS real time	MODIS-detected hot spots, processed by prep-chem-source model, mass-conserved normalization	1°×1°, 12 h	1 km × 1 km, 24 h
Top and Lateral Boundary Conditions	RAQMS real time (gases) + STEM tracer (several aerosols)	STEM 60 km base case	2°×2°, 6 h & 60 km×60 km, 6 h	60 km×60 km, 18 layers, 6 h

Ozone and sulfur oxides levels over California

M. Huang et al.

Title Page

Abstract | Introduction

Conclusions | References

Tables | Figures

◄◄ | ►►

◄ | ►

Back | Close

Full Screen / Esc

Printer-friendly Version

Interactive Discussion

Table 2. Modeled O_3 sensitivity along flight paths below 1 km from both resolution cases.

12 km	Biogenic			Fire		
Flight day	Mean (%)	Max (%)	Number of points with sensitivity > 10%/total number of points (%)	Mean (%)	Max (%)	Number of points with sensitivity > 10%/total number of points (%)
June 18 SC	1.36	4.98	0	0.28	0.65	0
June 20 SC	–	–	–	–	–	–
June 22 SC	1.64	3.73	0	2.81	13.72	5
June 24 SC	5.04	8.87	0	14.47	26.55	62.50
all SC	2.3	8.87	0	4.26	26.55	16.14
all CA	2.84	19.87	1.98	4.78	30.2	19.85
June 18 SC	6.04	26.5	15.7	3.19	25.65	5.38
June 20 SC	–	–	–	–	–	–
June 22 SC	1.63	5.57	0	2.05	6.2	0
June 24 SC	1.48	3.92	0	5.43	17.04	15.38
all SC	3.8	26.5	7.85	3.41	25.65	6.28
all CA	5	26.78	9	5.34	26.1	13

Table 3. Correlation (R), Mean Biases (MB), Root Mean Square Error (RMSE) between modeled and observed SO_x along all SC flight tracks. Higher correlations, lower MB and RMSEs are in bold.

Measurements	R (observations vs. predictions)		Observed Mean (ppb)	Mean Biases (ppb)		RMSE (ppb)	
	12 km Base	60 km Base		12 km Base	60 km Base	12 km Base	60 km Base
CIT SO_2	**0.36**	0.28	1.08	**0.41**	1.02	**1.55**	1.87
GIT SO_2	**0.43**	0.20	0.62	**0.13**	0.57	**0.81**	1.02
UNH SO_4	**0.54**	0.28	0.53	**0.30**	0.47	**0.39**	0.54
CUB SO_4	**0.50**	0.22	0.45	**0.22**	0.39	**0.40**	0.54

Ozone and sulfur oxides levels over California

M. Huang et al.

Table 4. Scaling factors determined by comparisons between 12 km simulations and observations.

	(flight time) all SC flight observed/ 12 km predicted	(24 h) surface observed/12 km predicted	Derived night time scaling factors
SO_2	1.71	1.35 (SC CARB)	1.09
SO_4	2.60	1.79 for 15:00–24:00 UTC 2.56 (Statewide CASTNET)	
Fine SO_4	3.17	2.5 (SC STN+IMPROVE)	2.02

Table 5. Air-mass properties below 1 km a.g.l. along three SC flight paths from observations and tracer calculations.

Flight day	VOC age (hour)	China CO (%)	North America CO (%)	SO$_4$-UNH (µg/sm^3)	SO$_4$-CUB (µg/sm^3)	SO$_2$-CIT (ppb)	SO$_2$-GIT (ppb)	SO$_4$ enhancements by foreign sources (µg/sm^3)	SO$_2$ enhancements by foreign sources (ppb)
June 18 SC	11.26	0.01	99.94	2.36	1.77	1.31	0.87	1.3×10^{-3}	6.5×10^{-4}
June 22 SC	10.73	0.2	99.74	2.16	2.29	1.37	–	6.0×10^{-3}	3.6×10^{-3}
June 24 SC	15.78	**16.61, (~40% 23:00–24:00 UTC)**	**78.42, (~40% 23:00–24:00 UTC)**	2.47	2.32	–	0.55	**0.53**	**0.12**

Table 6. Maximum and mean SO$_x$ emission rates over California and SC from both EIs and their top emissions sectors.

		Maximum (mole/km^2/day)	Mean (mole/km^2/day)	Top emission sector
CARB	Statewide	72	0.12	Ships and commercial boats, 52.1%
	SC	72	1.1	Ships and commercial boats, 44.6%
NEI	Statewide	226.2	0.17	Fossil fuel combustion, 51.3%
	SC	0.92	0.06	Non-road equipment, 40.4%

– The sector emissions ranks in CARB and NEI documentations are for summertime South Coast Basin and yearly Los Angeles County, respectively, not the same as our SC domain.

– Data sources: http://www.epa.gov/air/emissions/so2.htm, http://www.arb.ca.gov/app/emsinv/t25cat/cat_top25.php.
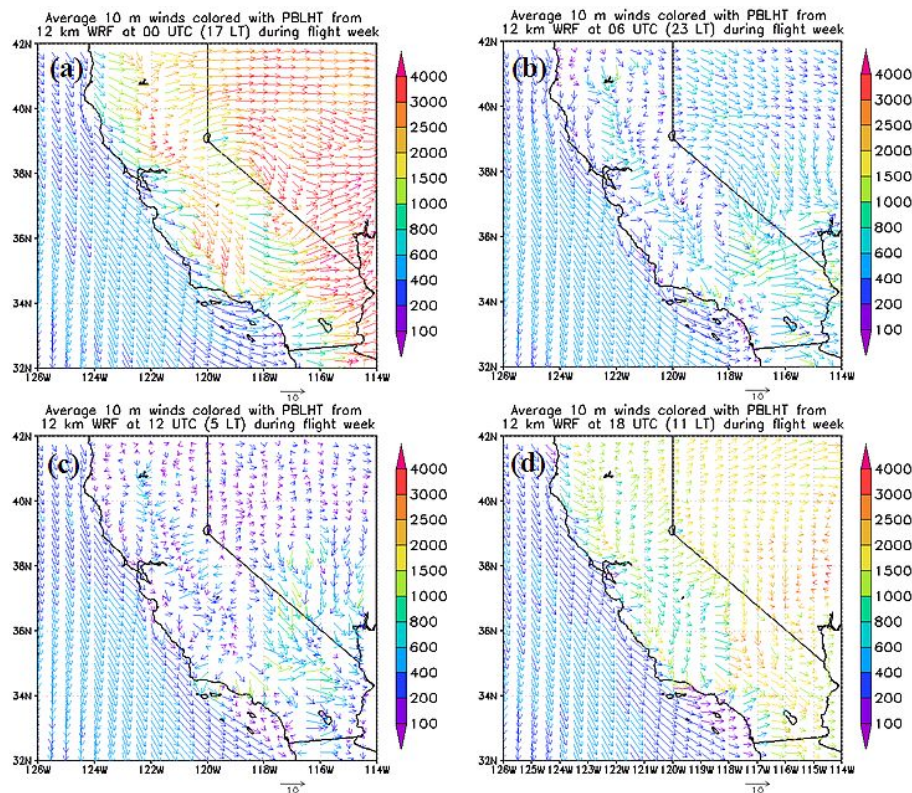
Fig. 1. Average 12 km WRF 10 m wind fields during the flight week, at **(a)** 00:00 **(b)** 06:00 **(c)** 12:00 **(d)** 18:00 UTC, colored by mixing layer height (m).
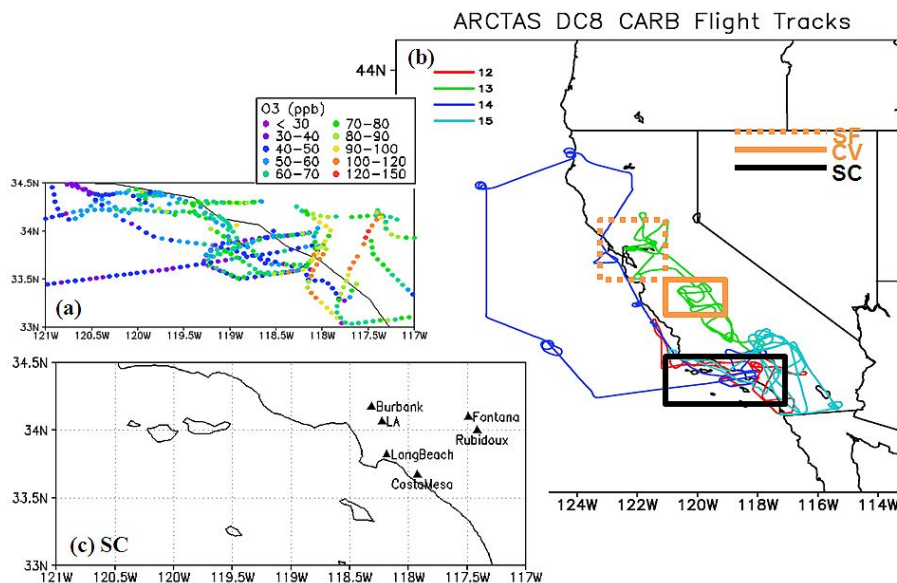
Fig. 2. (a) Observed O_3 along all SC flight path below 1000 m. **(b)** DC-8 flight 12–15 (on 18, 20, 22, 24 June) paths during ARCTAS-CARB period. **(c)** The locations of six SC surface sites.
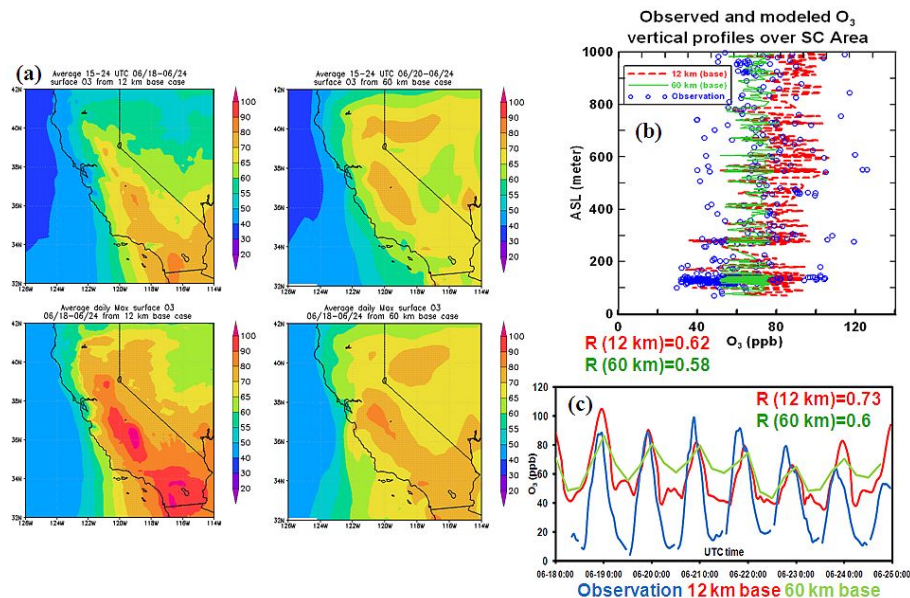
Fig. 3. (a) 12 km and 60 km modeled average flight time and daily maximum surface O$_3$ (ppb). **(b)** Observed and modeled O$_3$ (ppb) vertical profiles along all SC flight paths below 1 km. **(c)** Observed and modeled O$_3$ (ppb) time series at six SC surface sites.

Full Screen / Esc
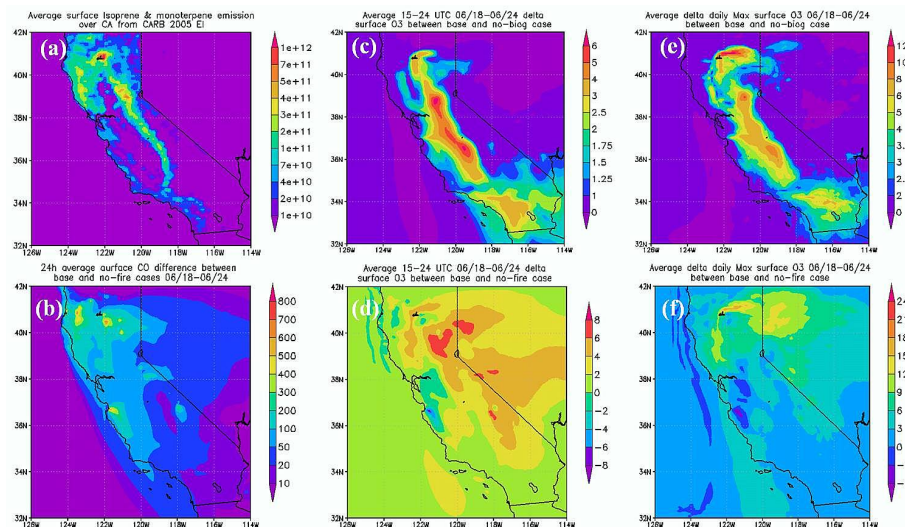
Fig. 4. **(a)** Average surface isoprene and monoterpene emissions (molecules/s/cm^2) from CARB EI. **(b)** Delta surface CO (24 h average) between base and no-fire cases in 12 km grids; delta surface O_3 (ppb) between **(c, e)** base and no-biog cases and **(d, f)** base and no-fire cases of **(c–d)** averaged 15:00–24:00 UTC and **(e–f)** average daily maximum O_3 (ppb) in 12 km grids.
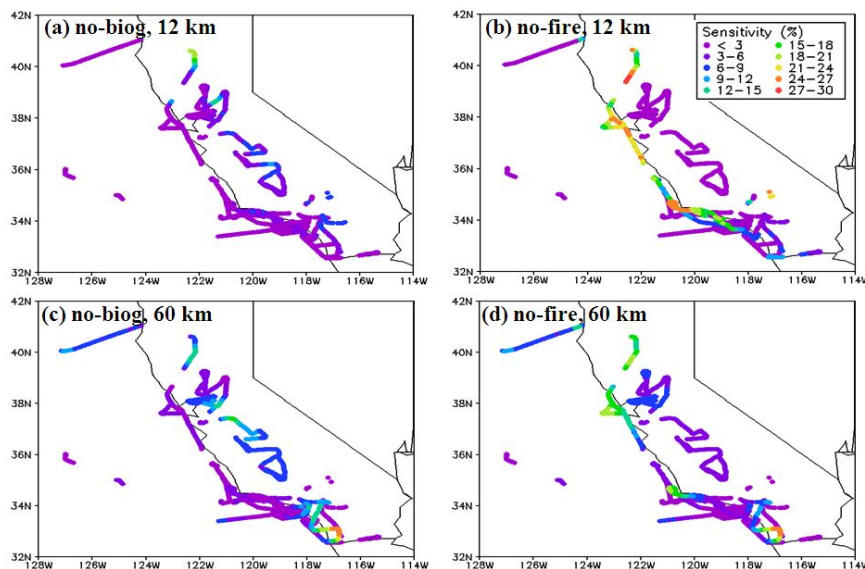
Fig. 5. Model sensitivity of O$_3$ for **(a, c)** no-biogenic case **(b, d)** no-fire case from 12 km (a–b) and 60 km (c–d) cases.

ACPD

10, 27777–27823, 2010

Ozone and sulfur oxides levels over California

M. Huang et al.

Title Page

Abstract | Introduction

Conclusions | References

Tables | Figures

◄ | ►◄

◄ | ►

Back | Close

Full Screen / Esc

Printer-friendly Version

Interactive Discussion
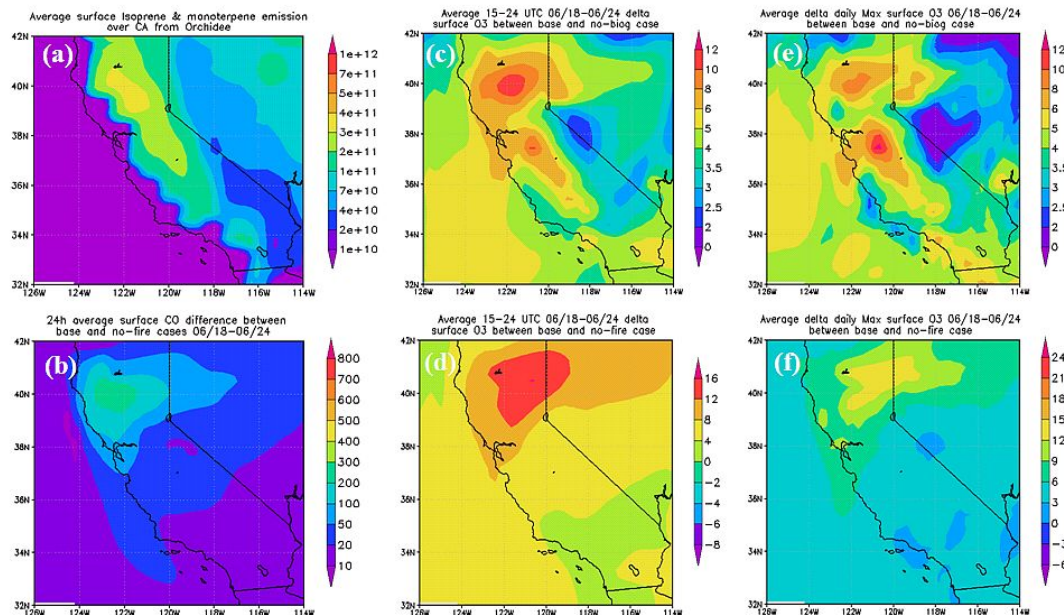
Fig. 6. (a) Average surface isoprene and monoterpene emissions (molecules/s/cm^2) from the Orchidee EI. **(b)** Delta surface CO (ppb, 24 h average) between base and no-fire cases in 60 km grids; delta surface O$_3$ (ppb) between **(c, e)** base and no-biog cases and **(d, f)** base and no-fire cases of (c–d) averaged 15:00–24:00 UTC and (e–f) average daily maximum O$_3$ (ppb) in 60 km grids.

Ozone and sulfur oxides levels over California

M. Huang et al.

Title Page

Abstract	Introduction
Conclusions	References
Tables	Figures

|◄   ►|

◄   ►

Back   Close

Full Screen / Esc

Printer-friendly Version

Interactive Discussion

M. Huang et al.

Title Page

Abstract	Introduction
Conclusions	References
Tables	Figures

◄◄	►►
◄	►
Back	Close

Full Screen / Esc

Printer-friendly Version

Interactive Discussion
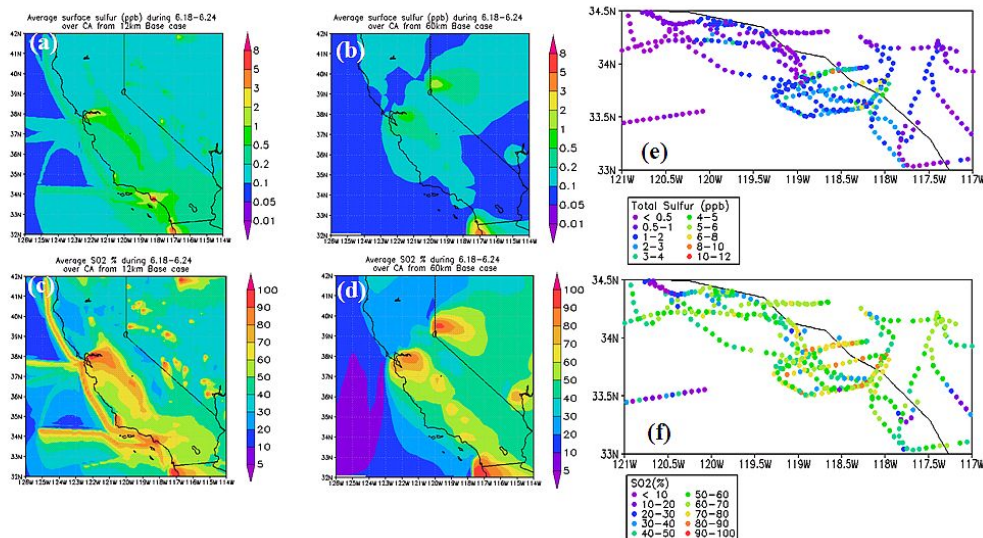
Fig. 7. The 24-h average surface **(a–b)** total sulfur (ppb) and **(c–d)** SO_2 % from 12 km (a, c) and 60 km (b, d) base simulations during flight week; Observed **(e)** SO_x and **(f)** SO_2 % along all SC flights below 1 km.
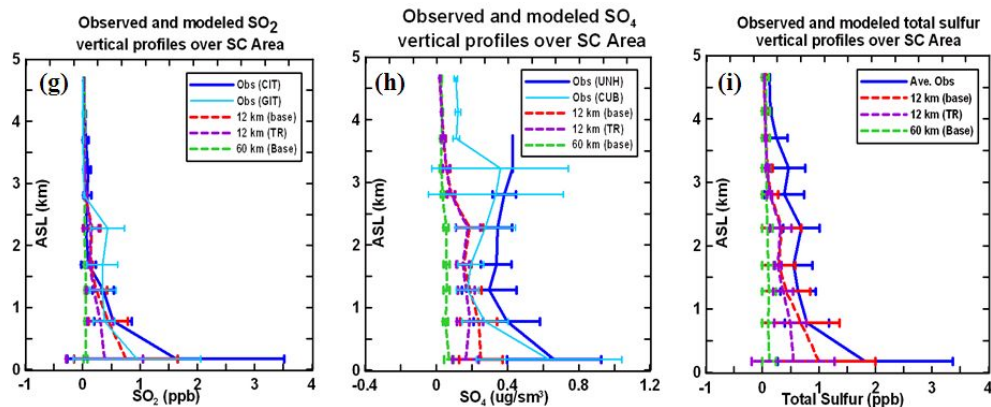
Fig. 7. Observed and modeled **(g)** SO_2 **(h)** SO_4 and **(i)** SO_x vertical profiles along all SC flights (averaged every 500 m).
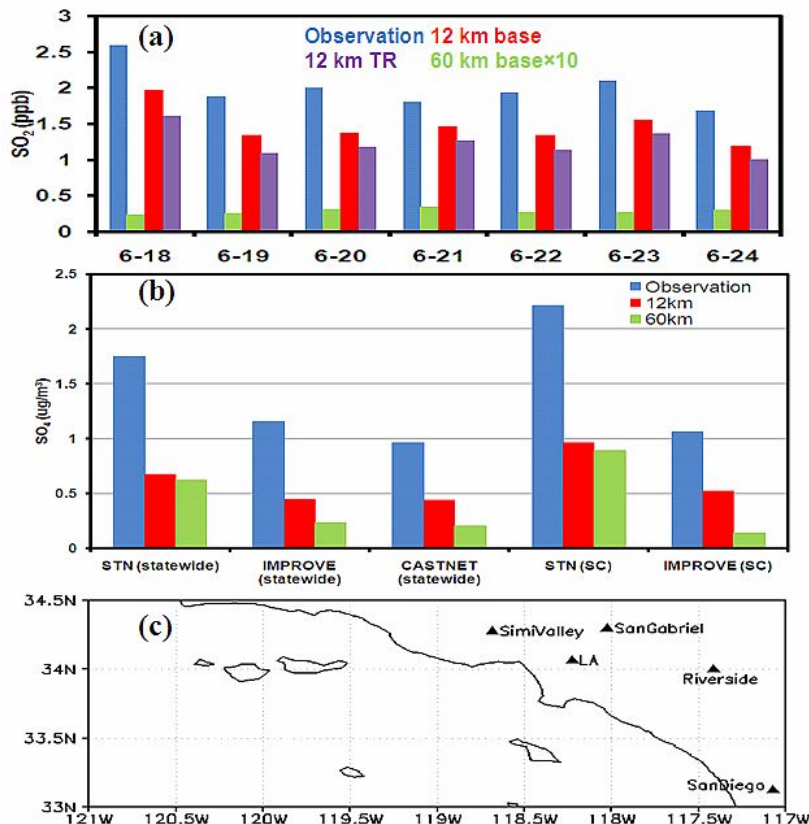
Fig. 8. (a) Daily-average (for six SC surface sites) observed and modeled SO_2. **(b)** Average observed and modeled fine SO_4 from STN and IMPROVE sites and total SO_4 from CASTNET sites during the flight week. **(c)** SC STN and IMPROVE sites locations.
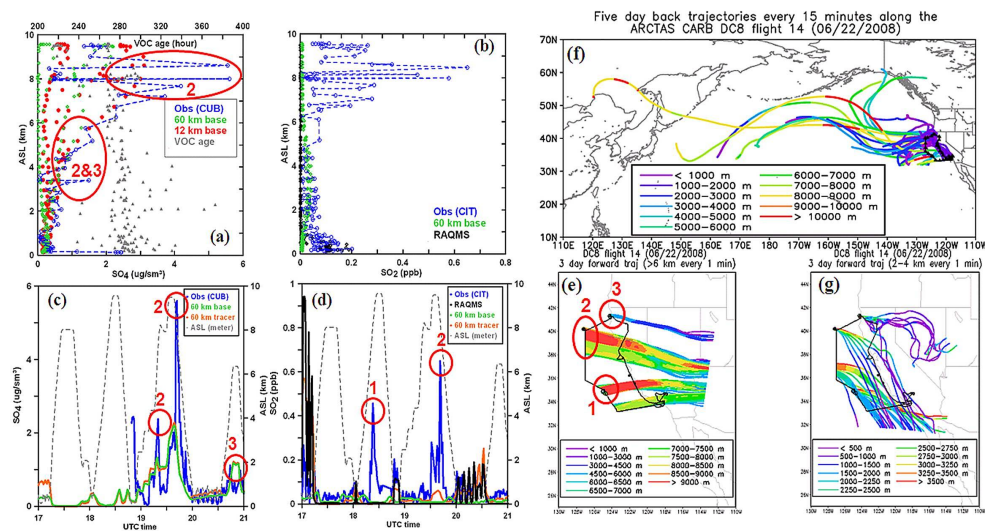
Fig. 9. Vertical profiles for **(a)** SO_4 and **(b)** SO_2 and time series for **(c)** SO_4 and **(d)** SO_2 along boundary layer flight on 22 June; **(f)** five-day back trajectories along this flight path. **(e)** Three-day forward trajectories (ASL>6 km) and **(g)** Three-day forward trajectories (a.s.l. between 2–4 km) along the 22 June flight path.
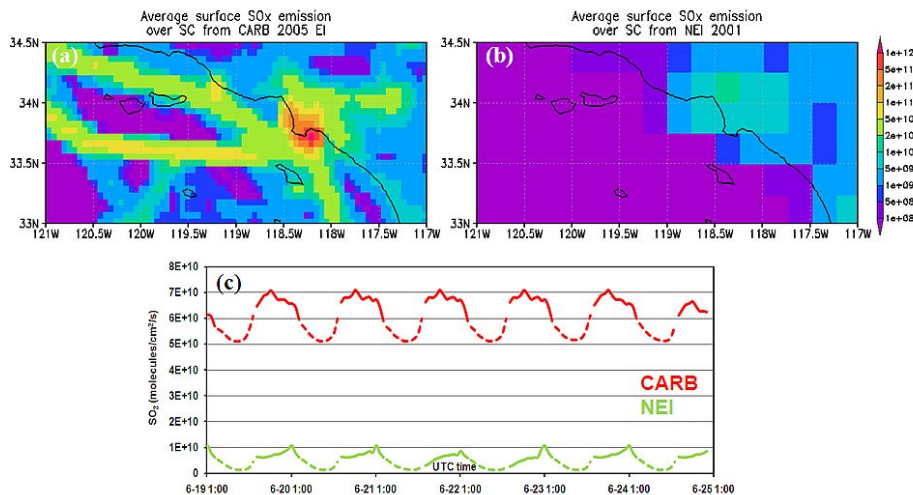
Fig. 10. The average surface SO_x (SO_2+PSO_4) emissions (molecules/s/cm^2) during 18–24 June over SC from **(a)** CARB EI and **(b)** NEI 2001; **(c)** SO_2 surface emissions from both EIs during 18–24 June over SC, solid and dash lines represent daytime (08:00 a.m.–08:00 p.m. Local Time) and night time, respectively.

Title Page

Abstract   Introduction

Conclusions   References

Tables   Figures

◄   ►

◄   ►

Back   Close

Full Screen / Esc

Printer-friendly Version

Interactive Discussion
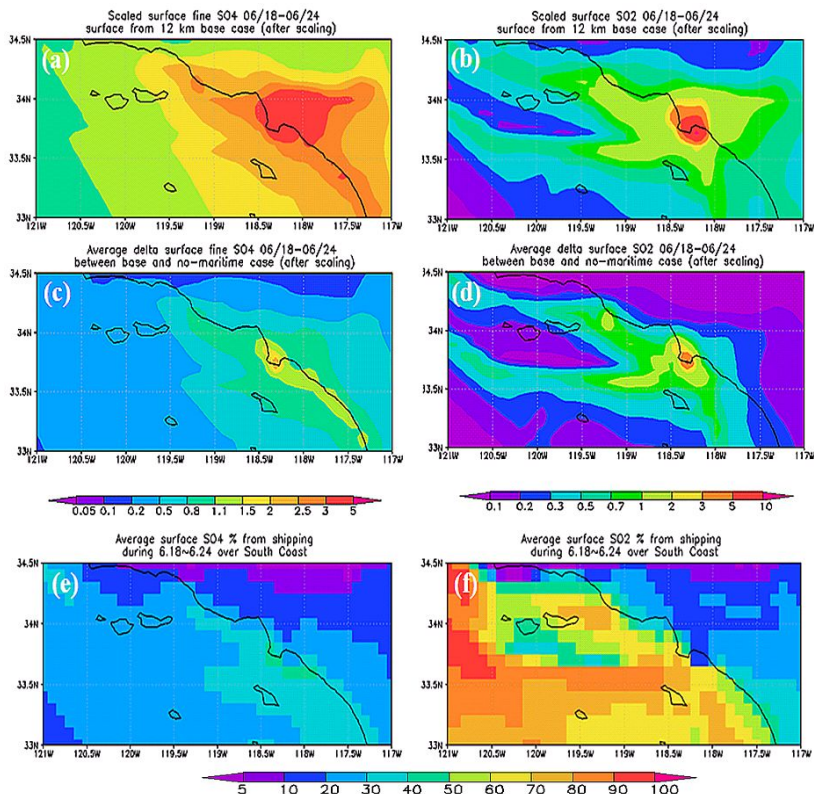
Fig. 11. The averaged surface 12 km base **(a)** fine SO_4 (µg/m^3) and **(b)** SO_2 (ppb) and contribution from maritime emissions for **(c)** fine SO_4 (µg/m^3) and **(d)** SO_2 (ppb) over SC during 18–24 June, after scaling; The 24-h averaged surface 12 km base **(e)** SO_4 % and **(f)** SO_2 % contributed from maritime emissions over SC.

Title Page

Abstract | Introduction

Conclusions | References

Tables | Figures

|◄ | ►|

◄ | ►

Back | Close

Full Screen / Esc

Printer-friendly Version

Interactive Discussion
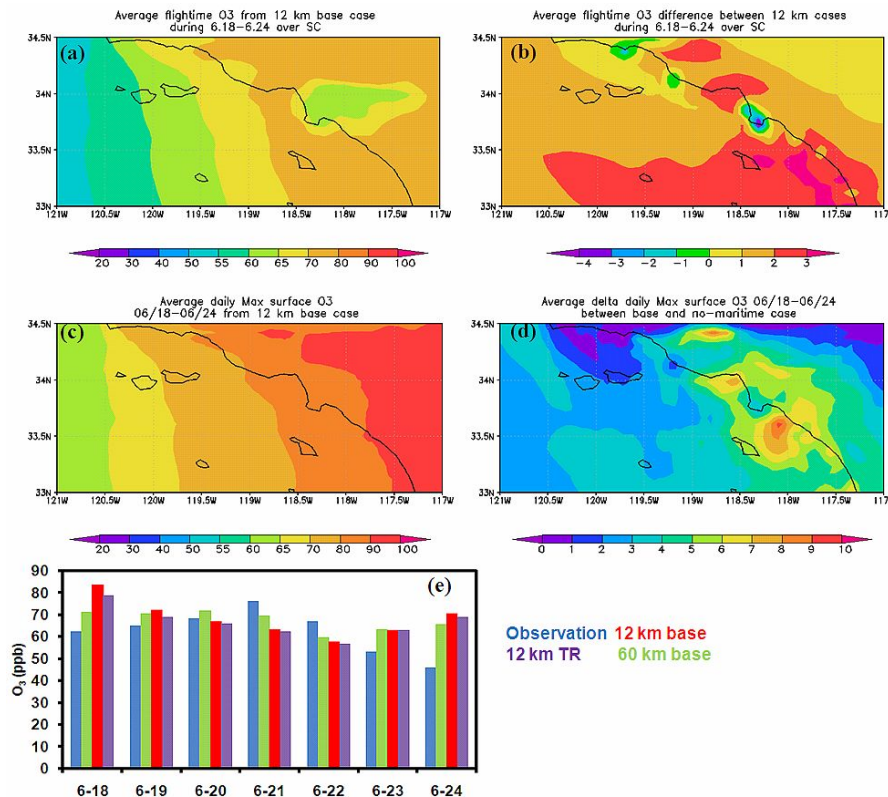
Fig. 12. (a) Flight-time average surface O$_3$ (ppb) from 12 km base case. **(b)** Flight-time average surface O$_3$ (ppb) differences between 12 km base and TR cases. **(c)** Average daily max. surface O$_3$ (ppb) from 12 km base case **(d)** Average daily max. O$_3$ (ppb) differences between 12 km base and TR cases during flight week **(e)** Daily-average (for six SC surface sites, flight time) observed and modeled O$_3$ (ppb).
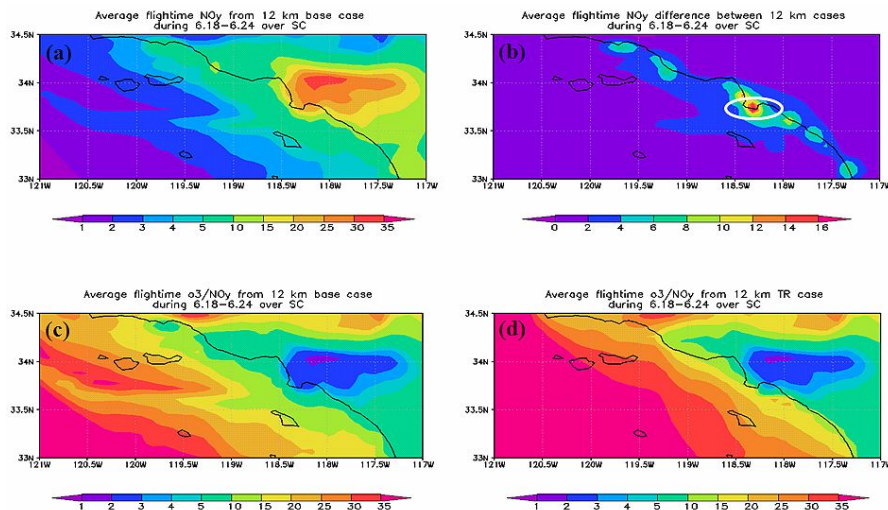
Fig. 13. **(a)** Flight-time average surface NO_y (ppb) from 12 km base case. **(b)** Flight-time average NO_y (ppb) differences between 12 km base and TR cases. **(c)** Flight-time average surface O_3/NO_y from 12 km base case, **(d)** Flight-time average surface O_3/NO_y from 12 km TR case.